2

High-Speed All-Optical Switches Based on Cascaded SOAs

Xuelin Yang, Qiwei Weng and Weisheng Hu
The State Key Laboratory of Advanced Optical Communication Systems and Networks, Shanghai Jiao Tong University, Shanghai, China

1. Introduction

Lots of research efforts have been focused to realize all-optical high-speed switches through nonlinear optical elements, for instance, high nonlinear fibers (HNLF), nonlinear waveguides as well as semiconductor optical amplifiers (SOAs). All-optical switches incorporating SOAs is one of the particularly attractive candidates due to their small size, high nonlinearities (low switching energy required) and ease of integration. All-optical switches also keep the network transparent, enhance the flexibility and capacity in network, and offer the function of signal regeneration, therefore SOAs provide various attractive all-optical functions in high-speed signal processing in fiber communication systems (Stubkjaer, 2000; Poustie, 2007), including all-optical AND/XOR logic gates, wavelength conversion (WC), optical-time division multiplexing (OTDM) de-multiplexing, optical signal regeneration and so on, which will be essential to the implementation of future wavelength division multiplexing (WDM) or optical packet switching (OPS) networks.

However, the operation speed of SOA based switches is inherently limited by its relative slow carrier lifetime (in an order of 100 ps) (Manning et al., 2007). Various schemes have been proposed to enhance the operation speed of SOA-based all-optical devices, for instance, 160 Gb/s and 320 Gb/s wavelength conversion was reported by using a detuned narrow band-pass filter to spectrally select one of the side-bands (blue-shifted or red-shifted) of the output signal (Liu et al., 2006, 2007). In this case, the SOA operation speed can be increased via the chirp effect on the SOA output associated with the SOA ultrafast gain dynamics. It has been shown that, the CW modulation response time has been reduced from 100 ps to 6 ps via filter detuning (Liu et al., 2006, 2007). Although using a detuned filter after the SOA can improve the optical signal-to-noise ratio (OSNR) of the output when comparing with the case of using a non-detuned filter (Leuthold, 2002), however the OSNR of the output signal will degrade to a large extent since the optical carrier was suppressed.

Recently, all-optical high-speed switches based on the cascaded SOAs were proposed and demonstrated. In Fig. 1, an all-optical switch incorporating two cascaded SOAs was proposed as an alternative high-speed technique, which was dubbed as "turbo-switch" (Manning et al., 2006; Yang et al., 2006, 2010), while preserving the OSNR of the output signal. An error-free wavelength conversion was demonstrated at 170 Gb/s (Manning et al., 2006). In addition, the operating speed of an all-optical XOR gate was also demonstrated at

85Gb/s, where dual ultrafast nonlinear interferometers (UNIs) were implemented (Yang et al., 2006, 2010) and the turbo-switch configuration was incorporated.

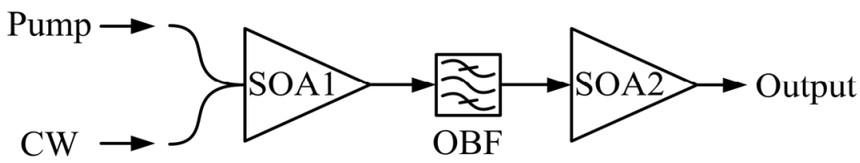

Fig. 1. Schematic setup of the turbo-switch, where the OBF is used to remove the pump signal. OBF: optical band-pass filter.

In this chapter, we will review the recent progress of the all-optical high-speed switches using cascaded SOAs, from both theoretical and experimental aspects. A majority of the publications (Manning et al., 2006, 2007; Yang et al., 2006, 2010) related to turbo-switch were reported, showing the high-speed experimental performances of turbo-switch over a single SOA. Apparently, a systematic theoretical turbo-switch model is necessary for the purpose of understanding the fundamental behaviors of the turbo-switch and how to further enhance the switch performance. First of all, we will present a detailed time-domain SOA model, from which the turbo-switches and switches with three or more cascaded SOAs can be evaluated. For the reason of convenience, we will refer hereafter to this kind of switch, including turbo-switch, as cascaded-SOA-switch. Then, we will focus on the relation between the overall performance of the switch and the nonlinear gain/refractive-index dynamics of the individual SOAs. The amplitude/phase dynamics of the optical output signal from the switch will be analyzed in details and compared with the experimental data. The SOA model will certainly help us not only to understand the basic principles of the switch, but also to exploit the way and the critical conditions for the switch to operate at even higher bit-rates.
The chapter is organized as follows. Section 2 presents a comprehensive theoretical analysis of the cascaded-SOA-switch, where the SOA model and the corresponding simulation method are presented. Simulation results including the gain/phase dynamics, pattern effect mitigation using turbo-switch, are shown in Section 3. Experimental demonstrations of 170 Gb/s AND gate (wavelength conversion) and 85 Gb/s XOR gate using turbo-switches are presented in Section 4. The cascaded-SOA-switches are further exploited in terms of the number of cascaded SOAs in Section 5, where the overall gain recovery time, the noise figure as well as the impact of injected SOA current of the cascaded switches are illustrated in details, as simulated by the model. Finally, conclusions will be given in Section 6.

2. Theoretical analysis of SOAs

To explore the operation principle and understand the performances of the cascaded-SOA-switch, a time-domain SOA model is required to analyze the fundamental gain/phase behaviors of the SOA-based device as well as to simulate the speed and application of the devices.

2.1 SOA model

The basic time-domain rate equations describing the carrier dynamics via the inter-band and intra-band processes in a single SOA, as proposed in (Gutiérrez-Castrejón, 2009; Mecozzi &

Mørk, 1997), are adopted. Travelling-wave equations in terms of the optical amplitude/power and phase, derived from Maxwell equations and Kramers-Kronig relations, are also incorporated in the SOA model to obtain the amplitude and phase of the output optical signal propagating through the SOA (Mecozzi & Mørk, 1997; Agrawal & Olsson, 1989).

Following the SOA model in (Mecozzi & Mørk, 1997), rate equations for the total carrier density N related to the (inter-band) band-filling effect, and the local carrier density variations n_{CH} and n_{SHB}, which are associated with the ultrafast (intra-band) effects: carrier heating (CH) and spectrum hole burning (SHB) processes respectively, can be expressed as follows:

$$\frac{\partial N(z,t)}{\partial t} = \frac{I}{eV} - R(N(z,t)) - v_g g S(z,t) - v_g g_{ase}\left[S^{+}_{ase}(z,t) + S^{-}_{ase}(z,t)\right] \tag{1}$$

$$\frac{\partial n_{CH}(z,t)}{\partial t} = -\frac{n_{CH}(z,t)}{\tau_{CH}} - \frac{\varepsilon_{CH}}{a_0 \tau_{CH}} g S(z,t) \tag{2}$$

$$\frac{\partial n_{SHB}(z,t)}{\partial t} = -\frac{n_{SHB}(z,t)}{\tau_{SHB}} - \frac{\varepsilon_{SHB}}{a_0 \tau_{SHB}} g S(z,t) - \left[\frac{\partial N(z,t)}{\partial t} + \frac{\partial n_{CH}(z,t)}{\partial t}\right] \tag{3}$$

where the first term in the right hand side (RHS) of (1) represents the increase of the total carrier density due to the injected current I to the SOA. Here, we have assumed a uniform distribution of the injected current along the longitude. In (1), e is the electron charge, and V is the volume of the active region in the SOA.

The radiative and nonradiative recombination rate due to the limited carrier lifetime in the SOA, $R(N)$ (Connelly, 2001), can be approached by,

$$R(N) = AN + BN^2 + CN^3 \tag{4}$$

where A, B, C represent the linear, bimolecular, and auger recombination coefficients respectively.

The third and fourth terms in the RHS of (1) are used to account for the depletion of total carrier density aroused from the stimulation emission by the injected light and the amplified spontaneous emission (ASE), respectively. v_g is the group velocity. g is the gain coefficient and S is the photon density in the active region. g_{ase} is the equivalent gain coefficient for ASE (Talli & Adams, 2003). τ_{CH} and ε_{CH} in (2) are carrier-carrier relaxation time and gain suppression factor caused by CH, while τ_{SHB} and ε_{SHB} in (3) are temperature relaxation time and gain suppression factor caused by SHB.

To take the gain dispersion into account better, and make our model applicable in a wide optical wavelength range, a polynomial model for the gain coefficient (Leuthold et al., 2000), which combines of a quadratic and a cubic function, is used, with one modification to include the ultrafast effect induced by CH and SHB.

$$g = \begin{cases} g_l + g_h, & \lambda < \lambda_z(N) \\ 0, & \lambda \geq \lambda_z(N) \end{cases} \tag{5a}$$

$$g_\beta = c_{N,\beta}\left[\lambda - \lambda_z(N)\right]^2 + d_{N,\beta}\left[\lambda - \lambda_z(N)\right]^3 \tag{5b}$$

where β = *l, h* represents the gain coefficient attributed to total carrier density N and CH/SHB effect, respectively.
Polynomial coefficients are calculated by,

$$c_{N,\beta} = 3\frac{g_{p,\beta}}{\left[\lambda_z(N) - \lambda_p(N)\right]^2} \tag{5c}$$

$$d_{N,\beta} = 2\frac{g_{p,\beta}}{\left[\lambda_z(N) - \lambda_p(N)\right]^3} \tag{5d}$$

where g_p, β, $\lambda_{p(N)}$ and $\lambda_{z(N)}$ stand for the material gain at the peak wavelength, the shifted wavelength at peak and transparency respectively. They are approximated by,

$$g_{p,l} = a_0(N - N_0) + \overline{a}a_0 N_0 e^{-N/N_0} \tag{5e}$$

$$g_{p,h} = a_0(n_{CH} + n_{SHB}) \tag{5f}$$

$$\lambda_p(N) = \lambda_{p_0} - \left[b_0(N - N_0) + b_1(N - N_0)^2\right] \tag{5g}$$

$$\lambda_z(N) = \lambda_{z_0} - z_0(N - N_0) \tag{5h}$$

where a_0, N_0, $\overline{a}$, λ_{p0}, b_0, b_1, λ_{z0}, and z_0 are parameters which have to be obtained by experimental gain dispersion curves (Leuthold et al., 2000). N_0 represents the transparency carrier density at the peak wavelength λ_0.
By definition, the photon density S (in unit of m^{-3}) in (1)-(3) can be expressed in terms of the light power P (in unit of W) as,

$$S(z,t) = \frac{P(z,t)}{h(c/\lambda)(\delta/\Gamma)v_g} \tag{6}$$

where h, c, δ, Γ denotes for Planck's constant, speed of light in vacuum, cross section area of the active region and confinement factor, respectively.
The travelling-wave equation of the input optical light (Agrawal & Olsson, 1989) is,

$$\frac{\partial P(z,t)}{\partial z} + \frac{1}{v_g}\frac{\partial P(z,t)}{\partial t} = (\Gamma g - \alpha_{\text{int}})P(z,t) \tag{7}$$

where the power P is a function of time t and position z along the active waveguide (z-axis) of the SOA. α_{int} is the internal loss in the active region. Eq. (7) only represents the positive direction propagation of the input light, since the facet reflection of the SOA (below 10^{-4}) is usually ignorable (Dutta & Wang, 2006).
For the propagation of the ASE power inside the amplifier, a bi-directional model presented in (Talli & Adams, 2003) is adopted, where the ASE is described by its total power while neglecting its spectral dependency. Equivalent coupling efficiency β_{ase}, equivalent wavelength λ_{ase}, and equivalent gain coefficient g_{ase}, are used in the calculation, for the reason of computational efficiency.

$$\frac{\partial P_{ase}^{\pm}(z,t)}{\partial z} \pm \frac{1}{v_g}\frac{\partial P_{ase}^{\pm}(z,t)}{\partial t} = \pm(\Gamma g_{ase} - \alpha_{\text{int}})P_{ase}^{\pm}(z,t) \pm \beta_{ase} R_{sp} \frac{hc}{\lambda_{ase}}\frac{\delta}{\Gamma} \tag{8}$$

where an additional term in the RHS, comparing to (7), is used to account for the spontaneous emission (SE) coupled into the effective waveguide. $R_{sp} = BN^2$ is the SE rate. "+" stands for the co-propagating direction with the input light, while "-" represents the counter-propagating direction.

Carrier density variations not only affect the gain, but also change the phase of the input optical signal. Associated with the gain dynamics through Kramers-Kronig relations, the phase shift (Mecozzi & Mørk, 1997) of the optical beam due to the SOA nonlinearity can be expressed as,

$$\frac{\partial \phi(z,t)}{\partial z} + \frac{1}{v_g}\frac{\partial \phi(z,t)}{\partial t} = -\frac{1}{2}\Gamma\left[\alpha_N g_l + \alpha_T g_{h,n_{SHB}=0}\right] \tag{9}$$

where α_N and α_T is the α-factors (also known as linewidth enhancement factor) for the band-filling and CH process, respectively. The subscript $n_{SHB} = 0$ means the SHB impact on the phase shift is ignored here.

It should be mentioned that, many physical effects of the SOA, including two-photon absorption (TPA), ultrafast nonlinear refraction (UNR), free-carrier absorption (FCA) and group velocity dispersion (GVD), are neglected in our SOA model. Ultrafast processes such as TPA, FCA and UNR are ignored reasonably, because these effects become important only when pulse energy is stronger than 1 pJ (Yang et al., 2003), while the pulse energy used in our simulation is generally lower than 0.1 pJ. GVD is also neglected, since the Gaussian pump pulsewidth (full width at half maximum, FWHM) in the paper is assumed to be 2~3 ps, which means that the spectral detuning from the central frequency is less than a few THz (Mecozzi & Mørk, 1997).

2.2 Numerical method

In order to solve the model numerically, we divide the SOA into N_z sections of equal length in the optical active waveguide, thus having a section length of $\Delta z = L/N_z$, and choose a corresponding time resolution of $\Delta t = \Delta z/n_g$. N_z should be large enough to have a good numerical approximation.

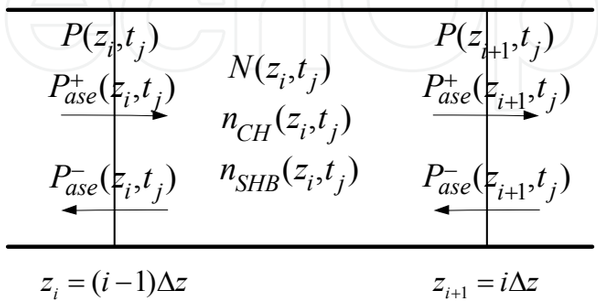

Fig. 2. A schematic sketch of the i^{th} section of the SOA.

Fig. 2 shows a sketch of the i^{th} section in the SOA, where i=1,2,…, N_z and j=1,2,…,N_t. N_z and N_t are the total number of the SOA sections and time steps respectively (Connelly, 2001).

Optical powers and ASE propagating in the positive and negative directions are calculated at the boundaries of each section, while the total carrier density and local carrier changes caused by the CH and SHB processes are considered at the center of each section. When the time interval Δt is small enough, the left hand side (LHS) of (1) can be approximated by,

$$\frac{\partial N(z_i,t_j)}{\partial t}=\frac{N(z_i,t_j)-N(z_i,t_{j-1})}{\Delta t} \tag{10}$$

Thus, basing upon the carrier density and the photon densities at the previous time step, we have,

$$\begin{aligned} N(z_i,t_j)=N(z_i,t_{j-1})+\Delta t\Bigg[&\frac{I}{eV}+R(N(z_i,t_{j-1}))-v_g g\frac{S(z_i,t_{j-1})+S(z_{i+1},t_{j-1})}{2}\\ &-v_g g_{ase}\frac{S^{+}_{ase}(z_i,t_{j-1})+S^{+}_{ase}(z_{i+1},t_{j-1})}{2}-v_g g_{ase}\frac{S^{-}_{ase}(z_i,t_{j-1})+S^{-}_{ase}(z_{i+1},t_{j-1})}{2}\Bigg] \end{aligned} \tag{11}$$

where a linear interpolation is employed to estimate the photon densities of the input optical beam, co-propagating and counter-propagating ASEs at the center of each section. Similar method can be applied to (2) and (3), to calculate the local carrier density variations due to CH and SHB processes.

The first term in the LHS of (7), describes the optical power propagating along the z-axis of the SOA, and experiencing an exponential amplification by a factor of (Γg - α_{int}), as shown in the RHS, which can be assumed constant in a sufficiently small interval Δz. The second term in the LHS, however, accounts for the optical power variation during the travelling time period in the section, which can be included using values obtained at last time step (Bischoff, 2004). Therefore, a solution of (7) is,

$$P(z_{i+1},t_j)=P(z_i,t_{j-1})\exp\left\{\left(\Gamma gN(z_i,t_{j-1})-\alpha_{\text{int}}\right)\Delta z\right\} \tag{12}$$

subjected to boundary condition,

$$P(z_1,t_j)=P_{in}(t_j) \tag{13}$$

where $P_{in}(t_j)$ denotes the input optical power at t_j.

Similar solutions can be given for the co-propagating and the counter-propagating ASEs, as described in (8),

$$P^{+}_{ase}(z_{i+1},t_j)=P^{+}_{ase}(z_i,t_{j-1})\exp\{g'_{ase}\Delta z\}+\left[\beta_{ase}R_{sp}(N(z_i,t_{j-1}))\frac{hc}{\lambda_{ase}}\frac{\delta}{\Gamma}\right]\frac{\exp\{g'_{ase}\Delta z\}-1}{g'_{ase}} \tag{14a}$$

$$P^{-}_{ase}(z_i,t_j)=P^{-}_{ase}(z_{i+1},t_{j-1})\exp\{g'_{ase}\Delta z\}+\left[\beta_{ase}R_{sp}(N(z_i,t_{j-1}))\frac{hc}{\lambda_{ase}}\frac{\delta}{\Gamma}\right]\frac{\exp\{g'_{ase}\Delta z\}-1}{g'_{ase}} \tag{14b}$$

where $g'_{ase}=\Gamma g(N(z_i,t_{j-1}),\lambda_{ase})-\alpha_{\text{int}}$, and subjected to boundary conditions respectively,

$$P^{+}_{ase}(z_1,t_j)=0 \tag{15a}$$

$$P_{ase}^{-}(z_{Nz+1}, t_j) = 0 \tag{15b}$$

where the facet reflection is neglected.

2.3 Simulation procedure

So far, we have presented a detailed model of a single SOA. The simulation of the cascaded-SOA-switch can be completed by the following calculation procedure, where we use the case of 2 SOAs (turbo-switch) as the example:

1. Calculate the steady state of SOA1, and obtain the initial state of the carrier densities, ASE in each section, which will be used as initial conditions in following calculations. In the case of the steady state, the RHS of (1)-(3) should equal to zero, which implies that the carrier densities in each section will keep unchanging if the input does not change. A numerical algorithm from (Connelly, 2001) is adopted here to give a good convergence.
2. Calculate the response of SOA1 and get the output, by applying a proper input optical signal like a pump pulse or a pseudo-random binary sequence (PRBS) modulated pump pulse train, in addition to the probe CW beam. Firstly, according to initial conditions at time step t_1 obtained from step 1), carrier densities $N(z_i, t_2)$ can be calculated by using (11), so does $n_{CH}(z_i, t_2)$, $n_{SHB}(z_i, t_2)$, and the optical signal and ASE power in each section at the time step t_2 from (12-15). Thereby, all necessary quantities of SOA1 at time step t_2 are obtained, which can be treated as initial conditions to further calculations of the next time step. As the iteration completes, the N and P at each section and each time step can be obtained, which gives the output of the SOA1, $P(z_{Nz+1}, t_j)$.
3. Filter out the pump pulse or PRBS, and only allow the modulated CW signal to enter the SOA2.
4. Repeat step 1) to get the initial steady conditions of SOA2 firstly. It should be mentioned that, under this circumstance the amplified CW after SOA1 has to be used as the input to SOA2 to obtain the initial carrier densities and ASE levels in each section of SOA2.
5. Repeat step 2) using the modulated CW signal from the output of SOA1, as the input to SOA2. Calculate the output of SOA2, which is the final output of the turbo-switch.

3. Simulation results

The parameters used in our model are list in Table I. Two identical SOAs are applied in all the turbo-switch simulation, as implemented in the reported experiments. The SOAs are 0.7 mm long, which have a relatively high gain and short carrier lifetime, as well as an acceptable noise figure. A 200 mA bias current is consistently used unless specifically described. A 100% of the injected current utilization is supposed in the model. In the following simulations, the input CW and pump pulse are at wavelengths of 1560 and 1550 nm respectively, and the pulsewidth is 3 ps (FWHM) if not otherwise specified.

A steady state numerical algorithm presented in (Connelly, 2001) is used to obtain the SOA gain saturation characteristics, as illustrated in Fig. 3, where the wavelength of the CW input beam is 1560 nm. It is shown that, the small-signal gain of the amplifier is 25 dB, while the saturation output power is 12 dBm.

Symbol	Description	Value
L	Length of active region	0.7 mm
δ	Cross section area of active region	0.2 μm^2
Γ	Confinement factor	0.45
I	Injected / Bias current of the SOA	200 mA
A	Linear recombination coef.	21×10^{8} /s
B	Bimolecular recombination coef.	10×10^{-16} m^3/s
C	Auger recombination coef.	35×10^{-41} m^6/s
v_g	Group velocity in the active region	8.5×10^{7} m/s
N_0	Transparency carrier density	0.65×10^{24} /m^3
a_0	Differential gain	3.13×10^{-20} m^2
$\overline{a}$	Gain model coef.	1.2
b_0	Gain model coef.	3.17×10^{-32} m^4
b_1	Gain model coef.	0
λ_{p0}	Wavelength at peak	1575 nm
λ_{z0}	Wavelength at transparency	1625 nm
z_0	Gain model coef.	-2.5×10^{-33} m^4
τ_{CH}	Temperature relaxation time	700×10^{-15} s
τ_{SHB}	Carrier-carrier scattering time	70×10^{-15} s
ε_{CH}	Gain compression factor due to CH	1×10^{-23} m^3
ε_{SHB}	Gain compression factor due to SHB	0.5×10^{-23} m^3
α_{int}	Internal loss	5000
β_{ase}	Equivalent SE coupling factor	3.65×10^{-4}
λ_{ase}	Equivalent ASE wavelength	1550 nm
α_N	α-factor due to band-filling	8.0
α_T	α-factor due to CH	1.0

Table 1. SOA parameters used in the simulation

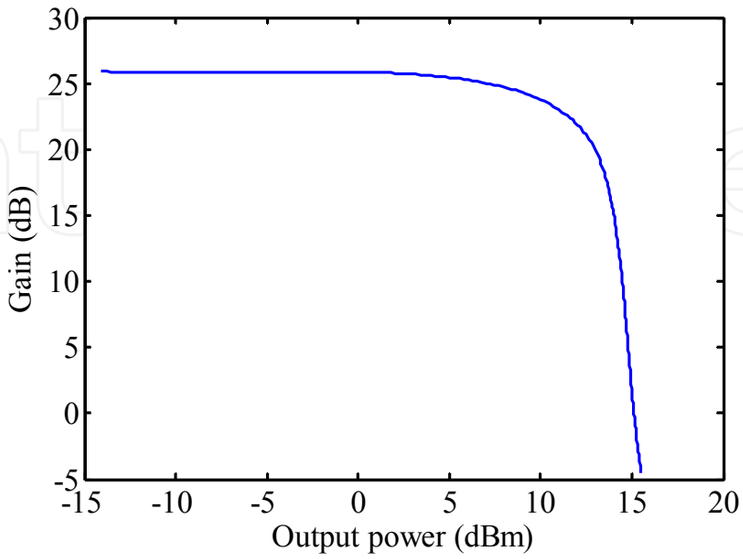

Fig. 3. Gain as a function of output power of a single SOA.

3.1 Gain and phase dynamics of turbo-switches

The gain dynamics of a single SOA and turbo-switch is plotted in Fig. 4. The input CW power is 0 dBm, while the pump pulse energy (single shot) is 100 fJ.

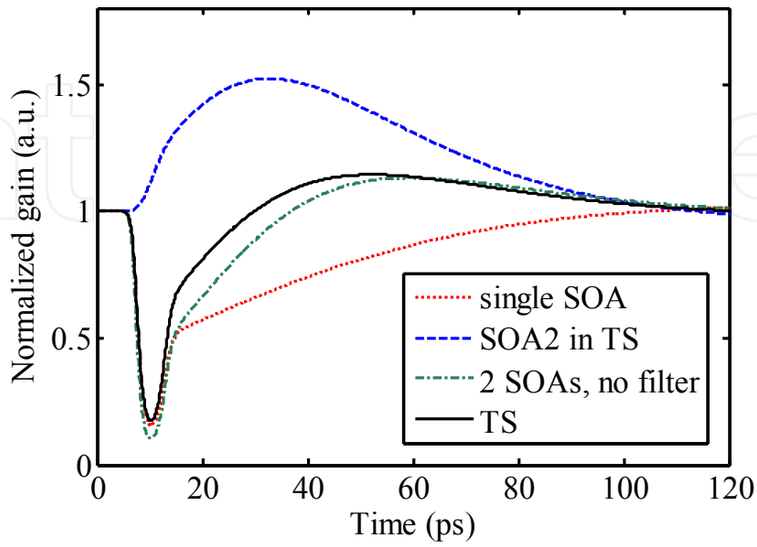

Fig. 4. Normalized gain of a single SOA, the SOA2 in TS, 2 cascaded SOAs with no filter between them, and the TS. TS: turbo-switch.

An obvious reduction of the gain recovery time is shown in the turbo-switch gain curve, comparing to the single SOA case, from about 100 ps to 20 ps, which is four times shorter than a single SOA. The simulation result is consistent with the corresponding experimental results presented in (Giller et al., 2006a). To get a better understand of the operating mechanism of turbo-switch, it is essential to know the gain response of SOA2, as plotted in Fig. 4. It is shown that, the gain curve of SOA2 has a completely different dynamics if compared with a single SOA. The gain of SOA2 increases firstly as the decrease of modulated CW input, and then starts to fall slowly back to the initial gain level. As a consequence, the slow recovery tail of the single SOA is somehow compensated, thus making the overall gain recovery of turbo-switch several times faster than that of a single SOA mechanism of turbo-switch, it is essential to know the gain response of SOA2, as plotted in Fig. 4. It is shown that, the gain curve of SOA2 has a completely different dynamics if compared with a single SOA. The gain of SOA2 increases firstly as the decrease of modulated CW input, and then starts to fall slowly back to the initial gain level. As a consequence, the slow recovery tail of the single SOA is somehow compensated, thus making the overall gain recovery of turbo-switch several times faster than that of a single SOA.

On the other hand, the phase dynamics curves are plotted in Fig. 5. It is shown that, turbo-switch also reduces the phase full recovery time from 100 ps to ~20 ps, about four times shorter than the case of a single SOA. It should be noted that the ultrafast effect of the SOA has much less impact on the phase change (Giller et al., 2006b), thus the phase recovery is mainly attributed to the inter-band processes, which makes it slightly different from the gain curve. To summarize, the turbo-switch scheme has shortened the overall gain/phase response time to a large scale compared with the case of a single SOA and has the capability of improving the overall operation speed of the switch to higher bit-rates.

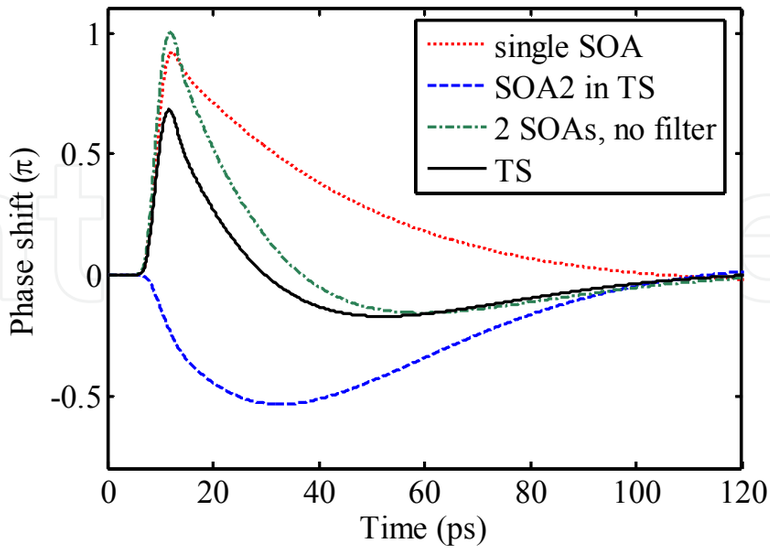

Fig. 5. Normalized phase dynamics of a single SOA, the SOA2 in TS, 2 cascaded SOAs with no filter between them, and the TS. TS: turbo-switch.

Moreover, our simulation shows that filtering the pump pulses before the SOA2 in turbo-switch scheme does further reduce the gain/phase recovery time, when compared to the case of no filter between two SOAs (dash-dotted gain/phase curves in Fig. 4), as presented in (Marcenas et al., 1995). In the latter case, the pump was entered into two cascaded SOAs along with the probe CW beam, which can also be regarded as a single long SOA with a double length of the active waveguide.

3.2 Pattern-effect mitigation of turbo-switches

As a result of the shorter gain/phase recovery time in turbo-switch, the pattern effect associated with the slow recovery is supposed to be mitigated. It should be noted that, along with the faster gain response of the turbo-switch, an overshoot in the gain/phase curve can also be clearly observed. However, the overshoot level can be controlled by adjusting the average input optical power to the SOA2. To verify the mitigation of the pattern effect, a variable optical attenuator (VOA) is experimentally applied before SOA2 in the turbo-switch configuration to optimize the output pattern of the turbo-switch (Giller et al., 2006c).

The simulation results of the turbo-switch gain dynamics under a single shot of 3 ps pump pulse are presented in Fig. 6, as a function of power levels before SOA2, which are in good agreement with the experimental results (see Fig. 6(b)) presented in (Giller et al., 2006c). In the simulation, the input CW power to SOA1 is 0 dBm and pump pulse energy is 100 fJ. It is shown that, when reducing the input power to SOA2, the recovery time becomes longer, and the level of the overshoot is lower. When the input power becomes low enough to make SOA2 unsaturated, the overall turbo-switch gain response will exhibit similar to that of a single SOA. So there is an optimum input power level for SOA2 in order to achieve the optimum effective recovery time at a specific data bit-rate.

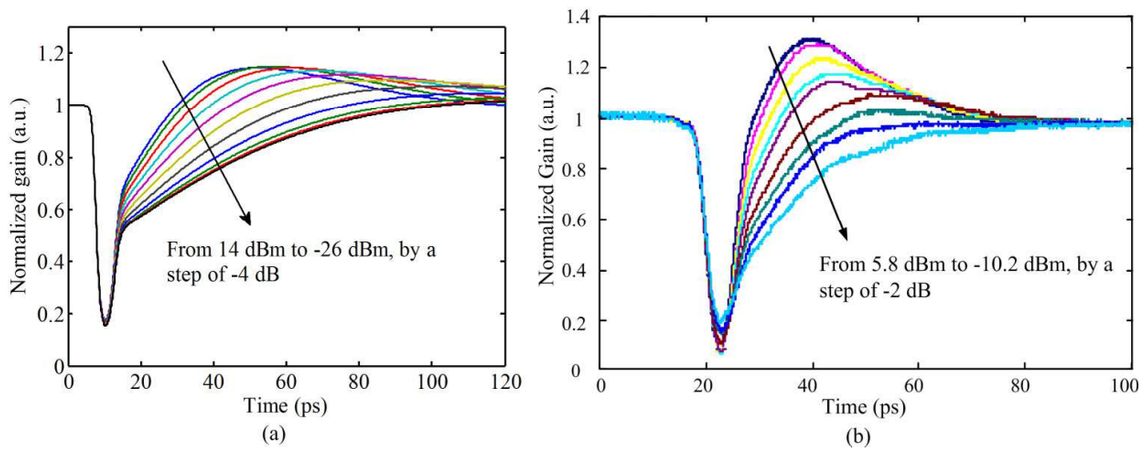

Fig. 6. Normalized gain dynamics of turbo-switch with a VOA before SOA2. (a).Simulation, where the optical power input to SOA2 varies from 14 to -26 dBm, by -4 dB each step. (b). Experimental result, where the optical power input to SOA2 varies from 5.8 to -10.2 dBm by a step of -2 dB (Giller et al., 2006c).

To show the pattern effect of turbo-switch, the output patterns of a CW probe beam modulated by a 40 Gb/s PRBS pump pulse train are presented in Fig. 7(a)-(c), where three different input power levels are chosen before SOA2: -26, -11, and 14 dBm. The input CW power before SOA1 is 0 dBm and the pump pulse energy is 2 fJ.

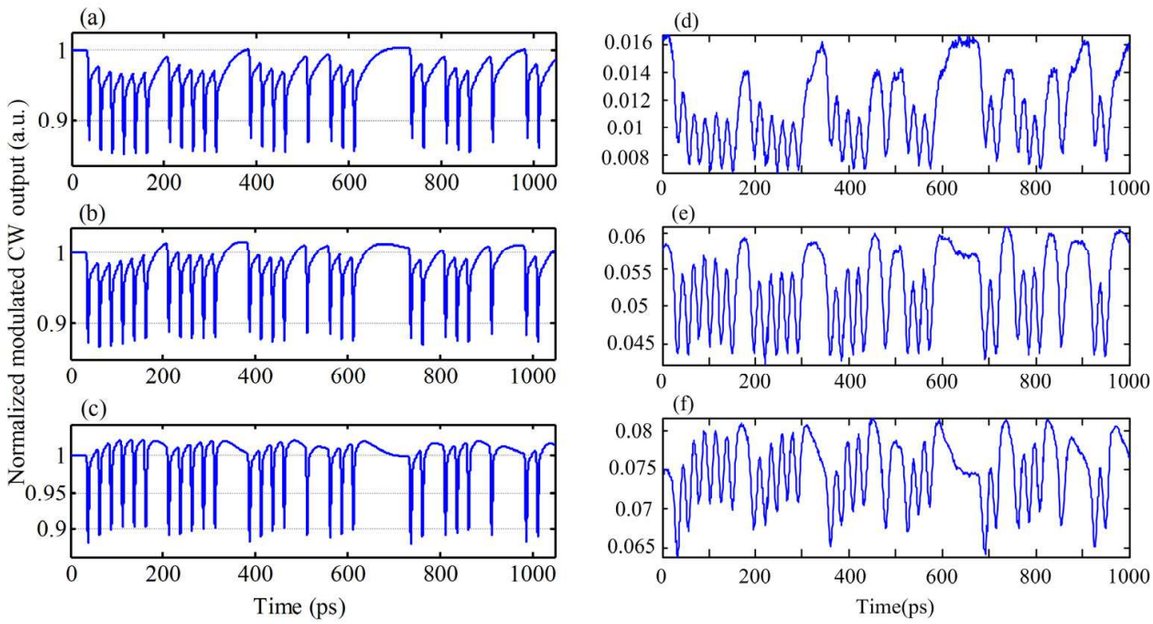

Fig. 7. Modulated CW output patterns from the TS, with a PRBS pump pulse train at 40 Gb/s. (a)-(c) Simulation, where, the optical power input to SOA2 in simulation are -26, -11 and 14 dBm respectively from top to bottom. (d)-(f). Experimental results (Giller et al., 2006c).

It is shown in Fig. 7 that, the simulation results are in good agreement with the experimental measurements (see Fig. 7(d)-(f)) presented in (Giller et al., 2006c) for all three cases.

Consequently, there is an optimum optical power level that could mitigate the pattern effect at a specific bit-rate. For instance, in this case, the optimum power to SOA2 should be -11 dBm, as shown in Fig. 7(b), where the pattern effect is mitigated.
On the contrary, the simulated modulation curves in Fig. 7(a) and 7(c) both experience a worse trend (constantly lower or higher) under a sequence of consecutive marks (ones) or spaces (zeros). This implies that, the unsaturated (-26 dBm), saturated (-11 dBm) and over-saturated (14 dBm) input power level to SOA2 has an important impact on the overall performance of turbo-switch. For instance, in the case of the modulated CW power of -26 dBm, the SOA2 cannot be saturated, and the overall recovery time is not shortened, turbo-switch behaviors similarly to a single SOA, as shown in Fig. 7(a).

4. Applications of turbo-switch

The turbo-switches are supposed to be applied in the all-optical signal processing in order to enhance the operation speed. The turbo-switches have been employed as the all-optical AND gate (wavelength conversion) and XOR gate, whose operation speeds have been increased up to 160 Gb/s and 85 Gb/s respectively. In this section, we will demonstrate the details of the high-speed operation of the turbo-switches, from both theoretical and experimental aspects.

4.1 High-speed AND gate beyond 160 Gb/s

The simulation results of the AND gate at 160 Gb/s will be given in Section 4.1.1, while the corresponding experimental results (i.e., wavelength conversion) at 170 Gb/s will be presented in Section 4.1.2.

4.1.1 Simulation of AND gate based on turbo-switch

A simulation was carried out to evaluate the 160 Gb/s all-optical wavelength conversion using a turbo-switch and a delayed interferometer (DI). The setup is shown in Fig. 8(a), where a polarization maintaining fiber (PMF) and a polarizer are used to form a DI (Reid et

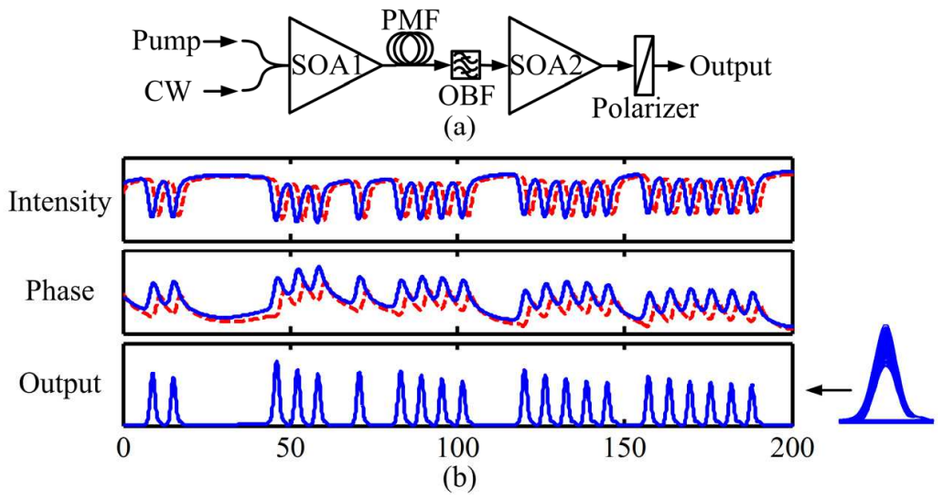

Fig. 8. All optical wavelength conversion using a turbo-switch. (a) Setup; (b) 160 Gb/s simulation results. The blue/ red curves are the TE/TM polarized components. Note that polarization controllers are not plotted for simplicity.

al., 2008). The DI utilizes the differential cross phase modulation (XPM) effect of the SOA to achieve the polarity-maintaining wavelength conversion. The PMF is used to introduce a delay between the TE / TM components of the probe, thus introducing a differential phase shift between the two orthogonal components. On the other hand, the polarizer acts as an interfering device to extract phase difference between the two components, which is the wavelength-converted output.

Fig. 8(b) presents the 160 Gb/s wavelength-converted output trace and the corresponding eye diagram. The average powers of the CW and the pump are 10 and 3 dBm respectively, while the wavelengths of the CW and pump are 1560 and 1550 nm respectively. The input PRBS data has a length of 2^7-1. The PMF gives a differential delay of 2 ps. It is shown that the turbo-switch configuration expedites the recovery of the intensity and phase, which helps to mitigate the patterning of the output. The clearly opening eye diagram of the output shows the feasibility of the wavelength conversion at 160 Gb/s. More specifically, the well-known Q factor, defined for instance in (Agrawal, 2002), for the output signal is 6.8, which corresponds to the bit error rate (BER) of 6.9×10^{-12}.

4.1.2 Experiment of AND gate based on turbo-switch

The wavelength conversion incorporating a turbo-switch was experimentally verified using the setup shown in Fig. 9(a), at ~85 and 170 Gb/s. The wavelength converter had the configuration of the DI. In a DI, CW light is amplitude and phase modulated in SOA1 by the action of the data pulse stream, and is then split into 'fast' and 'slow' components that travel along the two axes of a length of PM fiber. The two components experience a differential delay, Δt (3ps, in our experiment). The phase difference between them results in a polarization rotation when they interfere at the polarizer, and hence switching of the CW beam occurs, with a non-inverted output. The wavelength-converted output was de-multiplexed down to 42.6 Gb/s using MZ modulators.

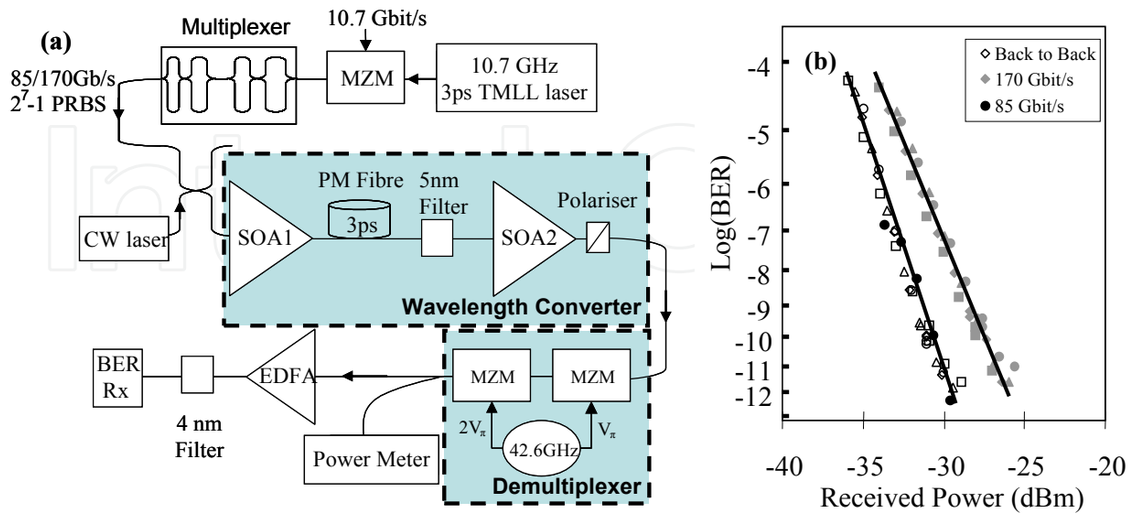

Fig. 9. 170 Gb/s wavelength conversion using DI configuration incorporating a turbo-switch. (a). The setup; (b). BER curves demultiplexed to 42.6 Gb/s for back-to-back and wavelength-converted signals at 85 and 170 Gb/s (Manning et al., 2006).

Fig. 9(b) shows the BER curves for the 42.6 Gb/s channels for wavelength conversion at 85 and 170 Gb/s. We observed no power penalty at 85 Gb/s, and a 3 dB penalty at 170 Gb/s, which we believe was due to the pulse width of the converted channels of 3 ps being slightly too long for 170 Gb/s data, and implied that our differential delay Δt is non-optimal. The measured OSNR was 40 dB, referred to a 0.1 nm noise bandwidth.

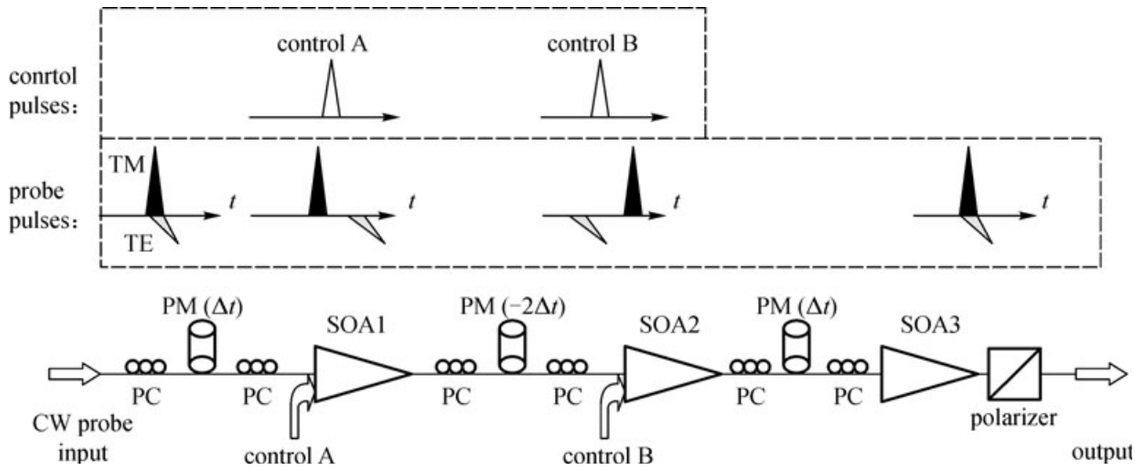

Fig. 10. Principle of dual-UNI XOR logic gate (PM: polarization maintaining fiber; PC: polarization controller)

4.2 High-speed XOR gate based on turbo-switch

Section 4.2.1 gives operation principle of the 85 Gb/s XOR gate, while the experimental results including eye diagram and the spectrum of the output are present in Section 4.2.2.

4.2.1 Principle of all-optical XOR gate

All-optical XOR logic is regarded as one of the fundamental logic gates in signal processing, which plays an important role in applications such as bit pattern recognition (Webb et al., 2009), pseudorandom bit sequence (PRBS) generation, parity checking and optical computing. A high-speed all-optical XOR gate has potential applications for on-the-fly digital serial processing of optical signals, for example, in packet header recognition, error detection and coding/decoding. In addition, the XOR function has been used recently as a wavelength converter and regenerator for signals in a differential phase shift keying (DPSK) format (Sartorius et al., 2006; Kang et al., 2005).

The scheme of the XOR logic gate is shown in Fig. 10. Two ultrafast nonlinear interferometer (UNI) elements are cascaded to allow two data pulse streams A and B to be input into SOAs 1 and 2 respectively as control pulses. The input probe pulses are launched into a polarization-maintaining (PM) fiber with equal intensities on the fast and slow fiber axes, which are coupled to the TM and TE axes of SOA1 respectively. As a result, the TE pulse lags the TM pulse by Δt. The control pulse A is introduced between the two probe pulse components before they are input into SOA1, in which it induces a π-radian phase shift experienced by the TE pulse alone. The probe pulses are then injected into another PM fiber with a differential delay of $-2\Delta t$. The fast and slow axes of this PM fiber are orthogonal to those of the first section, resulting in a reversal of the delay between TE and TM pulses so that the TE pulse is now Δt ahead of the TM pulse. The control pulse B is then introduced

between the TE and TM probe pulses before entering SOA2 where now the induced π-radian phase shift affects only the TM pulse. The third PM fiber, with differential delay, Δt, resynchronizes the TE and TM probe pulses in time. A π-radian phase shift between TE and TM pulses gives a polarization rotation of $\pi/2$ when they recombine at the polarizer, which is crossed with respect to the un-rotated probe.
When both of the control pulses A and B are present, the nonlinear phase difference between TE and TM will be zero (first π, then - π), the same result as the case when both A and B are absent. In the cases of either A or B alone being present, the phase shift will be ±π. The system is biased OFF (no output) in the absence of the control pulses. A pulse is generated after the polarizer only when one of A and B is present. Thus the operation of the device satisfies the XOR logic truth table as shown in Table 2. As with the conventional UNI gate, the probe pulses may be replaced by a continuous wave (CW) beam, in which case the output takes the form of pulses of width Δt.

Data A	Data B	XOR
0	0	0
0	1	1
1	0	1
1	1	0

Table 2. Truth table of XOR gate

The transmission of control pulse A is blocked by a filter (not shown) placed before SOA2. SOA1 and SOA2 are therefore configured as a turbo-switch (Manning et al., 2006) and the effective switching speed by control pulse A is enhanced. The addition of a third SOA (also after a filter) to the original dual ultrafast nonlinear interferometer XOR gate (DUX) forms a second turbo-switch that similarly enhances the speed of switching by control pulse B.

4.2.2 Experiment of XOR gate based on turbo-switch

An experiment was carried out to evaluate the performance the proposed XOR scheme at 85 Gb/s, whose experimental setup is shown in Fig. 11. A CW laser with a wavelength of 1552 nm was employed as the probe beam instead of a pulse train, so the first PM fiber in Fig. 10 was not required. The 3 ps, 1557 nm control pulses A and B were obtained from a 10.645 GHz mode-locked laser The control pulse stream was optically modulated with a 2^7-1 pseudo-random bit sequence (PRBS) and the pulses were passively multiplexed to 85 Gb/s before being injected into the SOAs 1 and 2. An optical delay-line was used to present different parts of the sequence to each SOA. Two variable optical attenuators (VOAs) were employed to adjust the control pulse energies. Another VOA was used to optimize the input power of the probe beam injected to SOA2.
All the three (Kamelian) SOAs were biased at 400mA, where their unsaturated gain was greater than 30 dB. The differential delays of PM fibers were 11.5 ps ($2\Delta t$) and 5.75 ps (Δt) respectively, where Δt is one half of the bit period at 85 Gb/s. 5 nm band-pass filters blocked the control pulses and allowed the propagation of the probe beam. The polarization controllers (PC) in front of each PM fiber were adjusted to launch approximately equal amplitudes into the TE and TM modes. The two polarization states were also aligned with the TE and TM modes of the active layer at the input to SOAs 1 and 2 with further PCs. This was to prevent the control pulses causing polarization rotation.

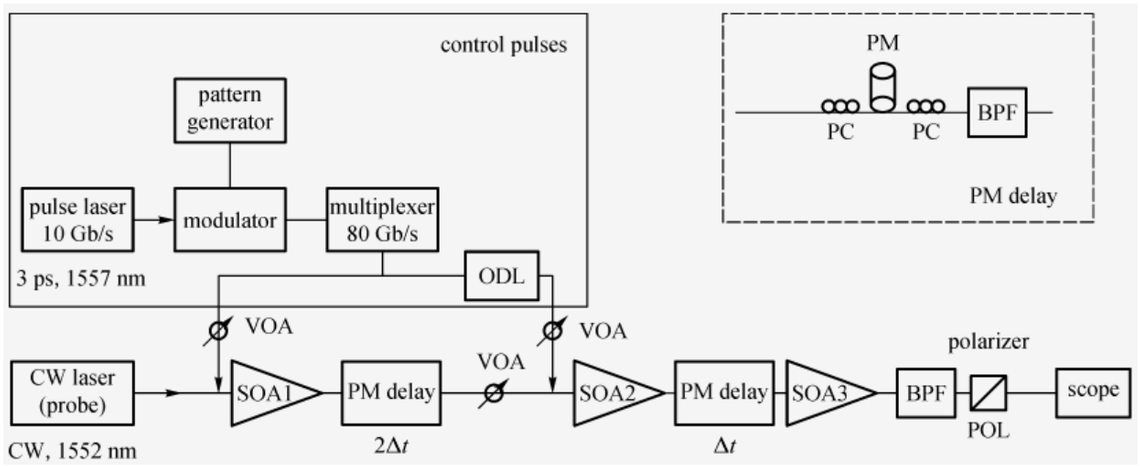

Fig. 11. Experimental setup of 85-Gb/s XOR logic gate, where PM delay indicates a length of PM fiber with PCs and a filter (inset).

The output of the XOR logic gate was monitored by a 70 GHz oscilloscope. XOR operation was realized at 10, 21, 42 and 85 Gb/s by adjusting the control pulse multiplexer. The amplitude variations in the 85 Gb/s output eye diagram (Fig. 12) were primarily due to imperfections in the multiplexer. The output spectrum at the same rate is shown in Fig. 13, where the sidebands are visible, but suppressed compared to a normal return-to-zero AND gate spectrum (The inset of Fig. 13). This is because the output pulses resulting from an $A \bullet \overline{B}$ input are in anti-phase to those corresponding to $B \bullet \overline{A}$. The average powers of the probe beam were 4 dBm before SOA1 and SOA2 and 10 dBm before SOA3. The average powers of control pulses A and B were 4 dBm and 3.5 dBm respectively, implying control pulse energies of 54 fJ and 62 fJ.

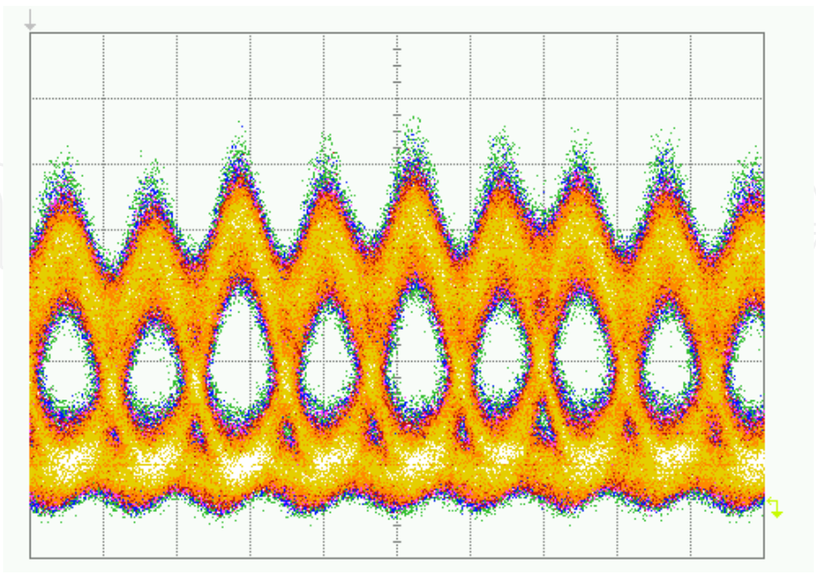

Fig. 12. 85 Gb/s XOR output eye diagram (5 ps/division).

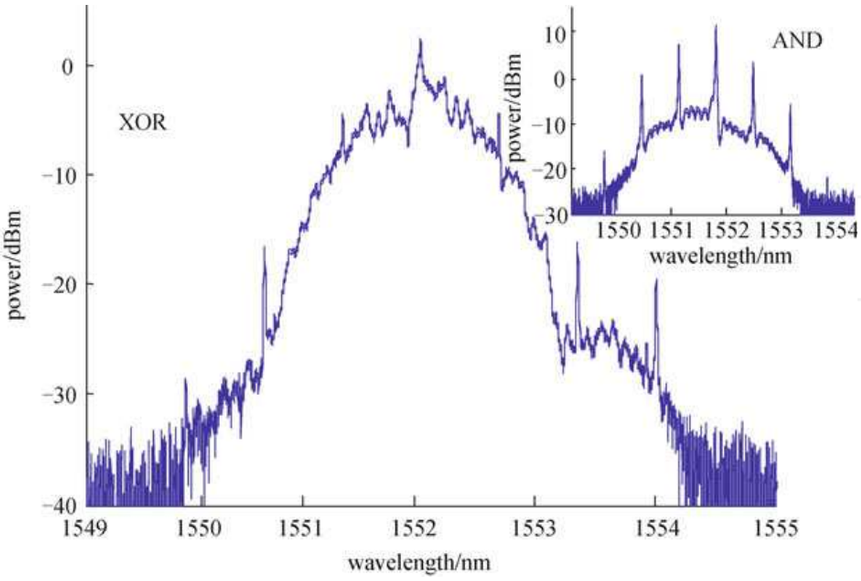

Fig. 13. Spectrum of 85 Gb/s XOR output (resolution is 0.01 nm; the inset is the corresponding spectrum of an 85 Gb/s AND gate)

5. Further improvement of the switch speed

In the turbo-switch structure, an extra SOA2 is cascaded following the SOA1, acting as a high-pass filter to filter out the slow response associated with the SOA carrier lifetime. In such a way, the overall operation speed of the turbo-switch device has been demonstrated several times faster than that of a single SOA. A straight-forward idea is that, if more SOAs are cascaded after the turbo-switch, is there any further improvement to the operation speed?

5.1 Switch of multiple cascaded SOAs

For the multiple cascaded SOAs, the simulations are carried out. The gain recovery time, overshoot level (normalized by the initial power level), and noise figure as a function of SOA stage are plotted in Fig. 14, where the powers of input CW probe and pump pulse to SOA1 are the same as Fig. 4. The noise figures of the cascaded switches are obtained using the equations presented in (Baney et al., 2000).

The results are actually encouraging, since the recovery time is reduced to ~10 ps when three SOAs are cascaded, which implies that more SOAs after turbo-switch, faster recovery could be expected. However, the degree of the overshoot and noise figure also rise almost linearly as the numbers of SOA increases, whereas the recovery time is not reduced significantly any more after the stage number exceeding 5. Moreover, the ASE noise and the complexity of the device are also expected to increase when more SOAs are cascaded. Therefore a trade-off has to be considered accordingly when choosing an optimum structure of turbo-switch for a specific application. Nevertheless, our simulation suggests that, the optimum number of SOA should be in the range of 2 to 5.

It should be mentioned that, SOAs can be cascaded directly without any filter between them as presented in (Marcenac & Mecozzi, 1997), where it requires ten SOAs to achieve a speed of 110 Gb/s, whereas our simulation shows that the same operation speed can be achieved with a three-SOA-switch if a filter is implemented, as indicated in Fig.14.

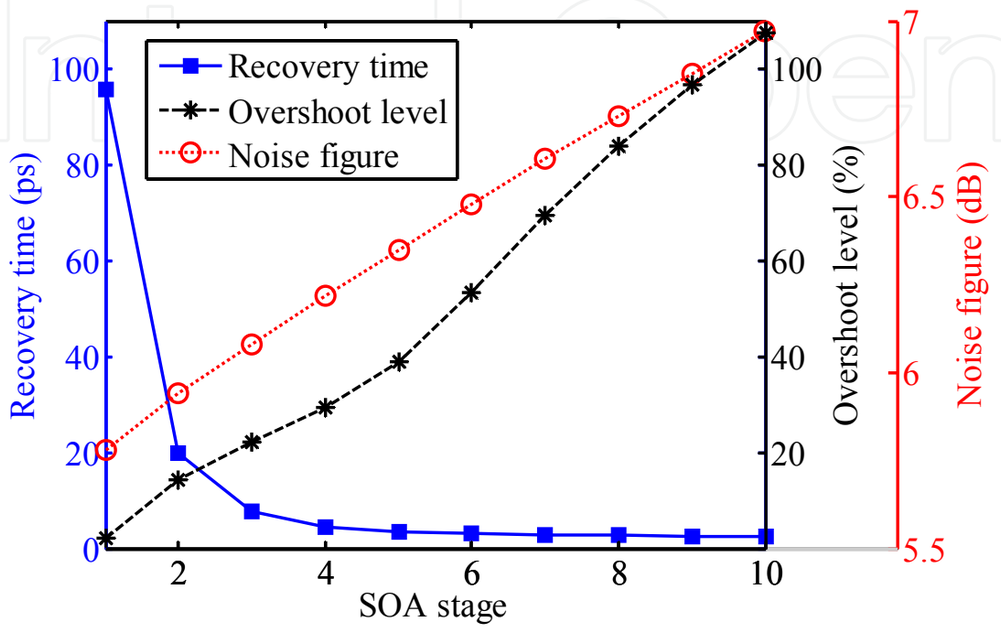

Fig. 14. Gain recovery time, overshoot level, and noise figure as a function of the number of the SOA stages.

5.2 Impact of SOA injected currents

For all the figures presented before this subsection, the SOA currents are fixed at 200 mA. Since the pattern effect can be mitigated using a VOA before the SOA2, as shown in Fig. 6. One could consider that whether the variation of the SOA current level can introduce a similar effect as the VOA? The simulation is carried out by varying one of the injected current of the SOA1 and SOA2 in turbo-switch scheme.

As shown in Fig. 15(a) and 15(b), the current variation curves reveal a similar effect as that of Fig. 6, where the nonlinearity of the SOA2 is gradually diminishing as the current keep decreasing, which consequently results in the overall response of turbo-switch similar to that of a single SOA. However, an interesting phenomenon is that, the gain dynamic is quite different when the current of SOA1 is reduced, as shown in Fig. 15(a). In the latter case, even though an overshoot is obvious when the current level is high, the full recovery time is generally longer than the case of Fig. 15(b). Apart from that, the gain compression induced by the pump pulse is smaller as well, which will potentially affect the extinction ratio (ER) of the output signal. To summarize, it is better to set the current level of SOA1 high, while the current level of SOA2 can be employed to optimize the overall gain/phase recovery time of the turbo-switch.

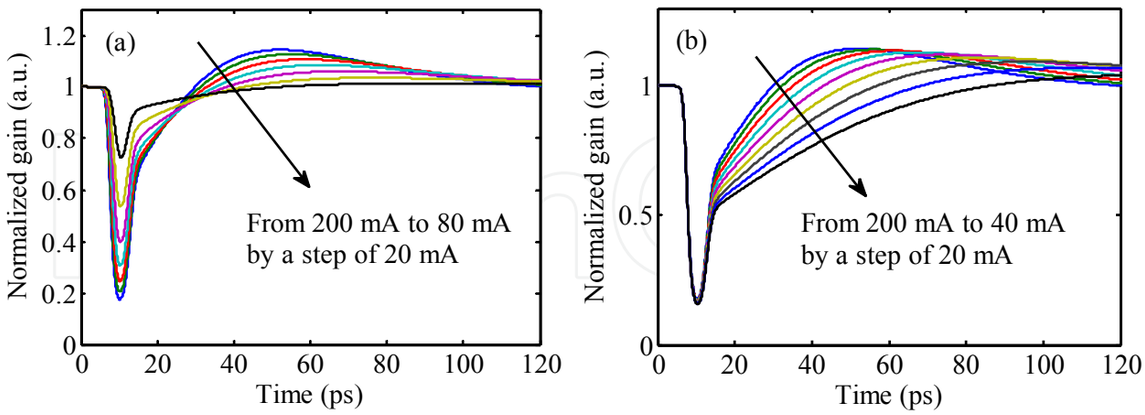

Fig. 15. Normalized gain dynamics of turbo-switch, by varying the injected current level of (a) SOA1, (b) SOA2.

6. Conclusions

A detailed theoretical model to simulate the gain/phase dynamics of the input optical signals propagating through turbo-switch has been presented. The simulation results have been shown in excellent agreement with experimental measurements incorporating the turbo-switch, in terms of CW modulation, pattern effect mitigation at 40 Gb/s, and eye diagram of 160 Gb/s wavelength conversion based on turbo-switch. The introduction of turbo-switch has the capability of increasing the overall switch speed by a factor of four if compared with the case of a single SOA switch, which is also confirmed by the previous experimental demonstration.

Moreover, the theoretical analysis based on the SOA model suggests that, higher bit-rate operation can be expected, if using an extended turbo-switch structure for instance with three or more cascaded SOAs. In addition, optimized configurations of turbo-switch with the differential XPM scheme as well as the bias current of SOAs can also be implemented to achieve a potential higher switch speed.

7. Acknowledgments

The authors would like to thank our colleagues Dr. R. J. Manning, Dr. R. P. Webb, and Dr. R. Giller from Tyndall National Institute, Ireland, for the experiment facilities and results used in the paper for comparisons.

8. References

Agrawal G. P. and Olsson N. A. (1989). Self-phase modulation and spectral broadening of optical pulses in semiconductor laser amplifiers. *IEEE J. Quantum Electron.*, vol. 25, no.11, pp. 2297-2306, ISSN 0018-9197.

Agrawal G. P. (2002). *Fiber-optic communication systems* (3rd edition), Wiley-Interscience, Wiley series in microwave and optical engineering, ISBN 978-0471215714,USA.

Baney D. M., Gallion P. and Tucker R. S. (2000). Theory and measurement techniques for the noise figure of optical amplifiers. *Opt. Fiber Technol.*,vol. 6, no. 2, pp. 122–154, ISSN 1068-5200.

Bischoff S., Nielsen M. L. and Mørk J. (2004). Improving the all-optical response of SOAs using a modulated holding signal. *J. Lightwave Techonol.*, vol. 22, no.5, pp. 1303-1308, ISSN 0733-8724.

Connelly M. J. (2001). Wideband semiconductor optical amplifier steady-state numerical model. *IEEE J. Quantum Electron.*, vol. 37, no. 3, pp. 439-447, ISSN 0018-9197.

Dutta N. K. and Wang Q. (2006). *Semiconductor optical amplifier*, World Scientific, ISBN 981-256-397-0, Singapore.

Giller R., Manning R. J. and Cotter D. (2006a). Recovery dynamics of the "turbo-switch". *Optical Amplifiers and Their Applications (OAA)*, Whistler, Canada, Jun. 2006. Paper OTuC2.

Giller R., Manning R.J. and Cotter D. (2006b). Gain and phase recovery of optical excited semiconductor optical amplifier. *IEEE Photon. Technol. Lett.*, vol. 18, no. 9, pp. 1061-1063, ISSN 1041-1135.

Giller R., Yang X., Manning R. J., Webb R. P. and Cotter D. (2006c). Pattern effect mitigation in the turbo-switch. *International Conference on Photonics in Switching*, Heraklion, Crete, Oct. 2006.

Gutiérrez-Castrejón R. (2009). Turbo-switched Mach-Zehnder interferometer performance as all-optical signal processing element at 160 Gb/s. *Opt. Commun.*, vol. 282, no. 22, pp. 4345-4352, ISSN 0030-4018.

Kang I., Dorrer C., Zhang L., Rasras M., Buhl L., Bhardwaj A., Cabot S., Dinu M., Liu X., Cappuzzo M., Gomez L., Wong-Foy A., Chen Y. F., Patel S., Neilson D. T., Jaques J. and Giles C. R. (2005). Regenerative all optical wavelength conversion of 40 Gb/s DPSK signals using a semiconductor optical amplifier Mach-Zehnder interferometer. *ECOC*, Glasgow, Scottland, Sep. 2005. Paper Th4.3.3.

Leuthold J., Mayer M., Eckner J., Guekos G., Melchior H. and Zellweger Ch. (2000). Material gain of bulk 1.55 mm InGaAsP/InP semiconductor optical amplifiers approximated by a polynomial model. *J. App. Phys.*, vol. 87, no. 1, pp. 618-620, ISSN 0021-8979 .

Leuthold J. (2002). Signal regeneration and all-optical wavelength conversion. *Annual Laser and Electro Optics Society (LEOS) Meeting 2002*, Glasgow, Scottland, Nov. 2002. Paper MM1.

Liu Y., Tangdiongga E., Li Z., Zhang S., Waardt H. de, Khoe G. D., and Dorren H. J. S. (2006). Error-free all-optical wavelength conversion at 160 Gb/s using a semiconductor optical amplifier and an optical bandpass filter. *J. Lightwave Technol.*, vol. 24, no.1, pp. 230-236, ISSN 0733-8724.

Liu Y., Tangdiongga E., Li Z., Waardt H. de, Koonen A. M. J., Khoe G. D., Shu X., Bennion I. and Dorren H. J. S. (2007). Error-free 320-Gb/s all-optical wavelength conversion using a single semiconductor optical amplifier. *J. Lightwave Techonol.*, vol. 25, no.1, pp. 103-108, ISSN 0733-8724.

Manning R. J., Yang X., Webb R. P., Giller R., Gunning F. C. G. and Ellis A. D. (2006). The turbo-switch—a novel technique to increase the high-speed response of SOAs for wavelength conversion. *OFC/NFOEC*, Anaheim, CA., Mar. 2006. Paper OSW8.

Manning R. J., Giller R., Yang X., Webb R. P. and Cotter D. (2007). SOAs for All-optical switching-techniques for increasing the speed. *International Conf. on Transparent Optical Networks*, Rome, Italy, Jul. 2007. pp. 239-242.

Marcenas D. D., Kelly A. E., Nesset D. and Davies D. A. O. (1995). Bandwidth enhancement of wavelength conversion via cross-gain modulation by semiconductor optical amplifier cascade. *Electron. Lett.*, vol. 31, no. 17, pp. 1442-1443, ISSN 0013-5194.

Marcenac D. and Mecozzi A. (1997). Switches and frequency converters based on cross-gain modulation in semiconductor optical amplifiers. *IEEE Photon. Technol. Lett.*, vol. 9, no. 6, pp. 749-751, ISSN 1041-1135.

Mecozzi A. and Mørk J. (1997). Saturation effects in non-degenerate Four-Wave mixing between short optical pulses in semiconductor laser amplifiers. *IEEE J. Sel. Topics Quantum Electron.*, vol. 3, no.5, pp. 1190-1207, ISSN 1077-260X.

Poustie A. (2007). SOA-based all-optical processing. *OFC/NFOEC*. Anaheim, CA., Mar. 2007. Tutorial-OWF1

Reid D. A., Clarke A. M., Yang X., Maher R., Webb R. P., Manning R. J. and Barry L.P. (2008). Characterization of a turbo-switch SOA wavelength converter using spectrographic pulse measurement. *IEEE J. Sel. Topics Quantum Electron.*, vol. 14, no. 3, pp. 841-848, ISSN 1077-260X.

Sartorius B., Bornholdt C., Slovak J., Schlak M., Schmidt C., Marculescu A., Vorreau P., Tsadka S., Freude W. and Leuthold J. (2006). All optical DPSK wavelength converter based on MZI with integrated SOAs and phase shifters. *OFC/NFOEC,* Anaheim, CA., Mar. 2006. Paper OWS6.

Stubkjaer K.E. (2000). Semiconductor optical amplifier-based all-optical gates for high-speed optical processing. *IEEE Journal of Selected Topics in Quantum Electronics*, vol.6, no.6, pp1428~1435, ISSN 1077-260X.

Talli G. and Adams M. J. (2003). Gain dynamics of semiconductor optical amplifiers and three-wavelength devices. *IEEE J. Quantum Electron.*, vol. 39, no.10, pp. 1305-1313, ISSN 0018-9197.

Webb R. P., Yang X., Manning R. J., Maxwell G. D., Poustie A. J., Lardenois S., Cotter D. (2009). All-optical binary pattern recognition at 42 Gb/s. *Journal of Lightw. Technol.*, vol. 27, no. 13, pp. 2240–2245, ISSN 0733-8724.

Yang X., Lenstra D., Khoe G.D. and Dorren H.J.S. (2003). Nonlinear polarization rotation induced by ultra-short optical pulses in a semiconductor optical amplifier, *Optics Comm.,* vol.223, no.1-3, pp.169-179, ISSN 0030-4018.

Yang X., Manning R. J. and Webb R. P. (2006). All-optical 85Gb/s XOR using dual ultrafast nonlinear interferometers and turbo-switch configuration. *ECOC*, Cannes, France, Sep. 2006. Paper Th1.4.2.

Yang X., Weng Q. and Hu W. (2010). High-speed, all-optical XOR gates using semiconductor optical amplifiers in ultrafast nonlinear interferometers. *Front. Optoelectron. China*, vol. 3, no. 3, pp.245–252, ISSN 1674-4128.

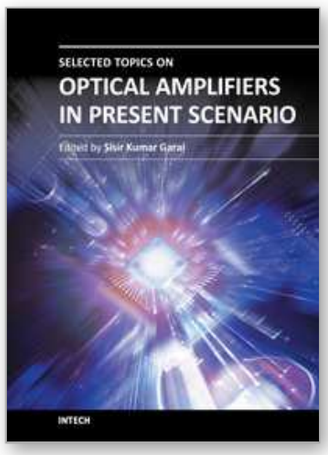

Selected Topics on Optical Amplifiers in Present Scenario

Edited by Dr. Sisir Garai

ISBN 978-953-51-0391-2
Hard cover, 176 pages
Publisher InTech
Published online 23, March, 2012
Published in print edition March, 2012

With the explosion of information traffic, the role of optics becomes very significant to fulfill the demand of super fast computing and data processing and the role of optical amplifier is indispensable in optical communication field. This book covers different advance functionalities of optical amplifiers and their emerging applications such as the role of SOA in the next generation of optical access network, high speed switches, frequency encoded all-optical logic processors, optical packet switching architectures, microwave photonic system, etc. Technology of improving the gain and noise figure of EDFA and, the study of the variation of material gain of QD structure are also included. All the selected topics are very interesting, well organized and hope it will be of great value to the postgraduate students, academics and anyone seeking to understand the trends of optical amplifiers in present scenario.

INTECH
open science | open minds

InTech Europe
University Campus STeP Ri
Slavka Krautzeka 83/A
51000 Rijeka, Croatia
Phone: +385 (51) 770 447
Fax: +385 (51) 686 166
www.intechopen.com

InTech China
Unit 405, Office Block, Hotel Equatorial Shanghai
No.65, Yan An Road (West), Shanghai, 200040, China
中国上海市延安西路65号上海国际贵都大饭店办公楼405单元
Phone: +86-21-62489820
Fax: +86-21-62489821

IntechOpen